DIRECT RECONSTRUCTION OF FIBRE ORIENTATION USING DISCRETE GROUND TRUTH INTERPOLATION

Bartosz P. Neuman[⋆∗] *Christopher Tench*[†] *Li Bai*[⋆]

[⋆] School of Computer Science, University of Nottingham, UK
[†] Academic Division of Clinical Neurology, University of Nottingham, UK

ABSTRACT

In this paper we present a novel approach to extracting fibre orientation information from the diffusion signal. We start the process by expanding the diffusion signal using spherical harmonics (SH) basis. In theory, this could lead to a mapping between SH coefficients and fibre orientations. In practice, finding such a mapping is non-trivial. Instead, we simulate the diffusion signal for a limited set of fibres (n different fibres with up to m fibre crossings) and store their corresponding SH coefficients in a database. We show that with such a database it is possible to find the precomputed fibre configuration closest to any SH expansion.

***Index Terms*—** diffusion weighted imaging, spherical harmonics expansion, fibre orientation reconstruction

1. INTRODUCTION

Magnetic Resonance Imaging (MRI) can produce excellent contrast of soft tissues and is thus an indispensable tool for visualising *in vivo* structural features of the human body for disease diagnosis and monitoring. Diffusion imaging is a special MRI modality which allows the use of information from the diffusion of water molecules in the brain to estimate fibre orientations, and reconstruct white matter tracts in the brain (tractography).

Diffusion weighted imaging can calculate a single scalar diffusivity, which depends on the direction of the applied magnetic field gradient, the diffusion sensitising gradient. The measured signal can be represented with an exponential model:

$$S_i = S_0 e^{-bADC_i}, \tag{1}$$

where S_0 is the amplitude of the measured signal with no diffusion sensitising gradients applied, S_i with the diffusion sensitising gradient applied at direction i, b a diffusion-weighting factor and ADC_i the apparent diffusion coefficient in the direction i. Diffusion tensor imaging (DTI) extends this 1D data and reconstructs the three-dimensional diffusion profile [1, 2] using a 2nd order tensor:

$$S_i = S_0 \exp(-b\vec{g}_i^{\mathrm{T}}\mathbf{D}\vec{g}_i), \tag{2}$$

∗Corresponding author (bartosz.neuman@nottingham.ac.uk).

with $\mathbf{D}$ being a diffusion tensor and $\vec{g}_i$ the direction of the diffusion sensitising gradient. Since $\mathbf{D}$ is a positive definite matrix (diffusion cannot be negative) and symmetric (water molecules are uncharged particles [2]), it has 6 unique elements. Therefore, in order to determine $\mathbf{D}$ at least six DW images are necessary. In practice, more than 6 images are taken in order to reduce the effect of low signal-to-noise ratio (SNR) of a single image [3]. The acquired samples should be evenly distributed to reduce the noise bias and to keep the statistical properties of the computed parameters rotationally invariant [4, 5, 3].

Although widely used, the single diffusion tensor model is inaccurate for more complex fibre configrations, such as multiple fibre crossing, kissing, and bending [6, 7, 8]. The diffusion signal within voxels containing multiple fibres can be explained as a sum of single tensors responses [9, 7]:

$$S_i = S_0 \sum_{k=1}^{n} v_k \exp(-b\vec{g}_i^{\mathrm{T}}\mathbf{D}_k\vec{g}_i). \tag{3}$$

$\mathbf{D}_k$ is a diffusion tensor of the kth fibre and v_k a volume fraction ($\sum_{k=1}^{n} v_k = 1$), which tells how strongly the fibre affects the total diffusion within the voxel. An n-fibre crossing will have $6n$ unique parameters, and to be correctly resolved requires at least that many different diffusion weighted images.

The protocol for obtaining the diffusion signal from many different directions is called high angular resolution diffusion imaging (HARDI) [10]. The measured diffusion signal is usually approximated with a truncated series of spherical harmonic (SH) basis functions. SHs can be seen as the extension of Fourier basis functions to the sphere, and are given by:

$$Y_l^m(\theta,\phi) = \sqrt{\frac{2l+1}{4\pi}\frac{(l-m)!}{(l+m)!}} P_l^m(\cos\theta)\exp(im\phi), \tag{4}$$

with P_l^m being the associated Legendre function of band (order) l and degree m. For practical reasons, a single integer $j(l,m) = l^2 + l + m$ is often used to enumerate the spherical harmonic series (SHS). Due to antipodal symmetry of diffusion, the odd order basis functions do not appear in

	#1	#2	#3	#4	#5	#6	#7	#8	#9	#10	#11
V	72	92	132	162	192	212	252	272	282	312	362
D	24.8	21.4	18.4	16.1	15.2	14.7	13	12.6	12.4	11.9	10.9
A	9.23	8.4	6.88	6.31	5.71	5.51	5.04	4.9	4.65	4.44	4.17
R	2.69	2.62	2.68	2.65	2.7	2.71	2.64	2.64	2.69	2.7	2.66

Table 1. Different spherical packings (databases) and their corresponding: (V) number of vectors, (D) the distance between any two neighbouring vectors, (A) average distance between random fibre and resolved fibre and (R) minimal to average distance ratio.

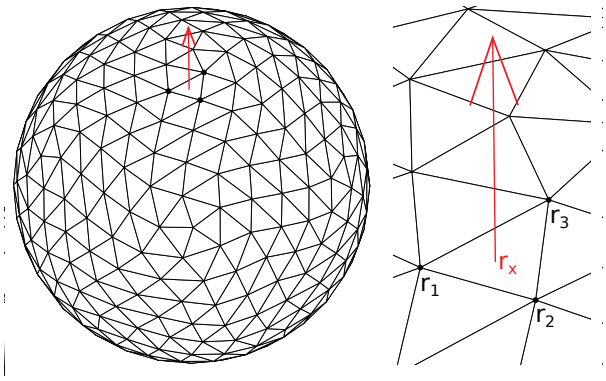


Fig. 1. Spherical sampling - vertices represent fibre directions for which the signal expansion is known. Unknown red fibre will be resolved as one of the neighbours.

Equation 4. The diffusion signal (Equation 3) can now be explained using spherical harmonics:

$$S(\theta,\phi) = \sum_j \alpha_j Y_j(\theta,\phi), \tag{5}$$

where α are SHS coefficients.

Unfortunately, with a generic representation of the signal it is no longer possible to directly infer the fibre configuration, so the diffusion signal is processed further. There are a number of methods that can be used to reconstruct the fibre orientations, including: two and multi-tensor models [11, 12, 13], higher order tensors [14], spherical deconvolution [15, 16], q-ball imaging [17, 18], diffusion orientation transform [19] and persistent angular structure MRI [20].

In this paper we present a novel method for direct fibre extraction based on HARDI data and a precomputed, discrete ground truth.

2. METHODS

Spherical harmonics are complete, global function that can be used to represent any spherical signal. When representing the diffusion signal though, the SH coefficients $\boldsymbol{\alpha}$ are drawn from a subspace of R^n. To learn the subspace of $\boldsymbol{\alpha}$, we have permuted the $\mathbf{D}$ over all possible leading directions $\vec{r}$ and looked at how $\boldsymbol{\alpha}$ changes in accordance to $\vec{r}$. This results in a mapping between $\vec{r}$ and $\boldsymbol{\alpha}$ based on Equations 3 and 5:

$$\sum_k v_k \exp(-b\vec{g}^{\mathrm{T}}\mathbf{D}_k\vec{g}) = \sum_j \alpha_j Y_j(\theta,\phi). \tag{6}$$

The diffusion signal is normalised by S_0 and the truncation of SH series on the right side is disregarded. Vector $\vec{g}$ is represented in Cartesian coordinates on the left and in polar coordinates (as θ and ϕ) on the right.

We observe that for any $\vec{r}$ and its signal expansion $\boldsymbol{\alpha}$ the $\vec{r}_x \subset (\vec{r}_1,\vec{r}_2,\vec{r}_3)$ will have its signal expansion $\boldsymbol{\alpha}_x \subset (\boldsymbol{\alpha}_1,\boldsymbol{\alpha}_2,\boldsymbol{\alpha}_3)$. Operator $\subset$ means that $\vec{r}_x$ is bound by vectors $\vec{r}_1,\vec{r}_2,\vec{r}_3$ (see Figure 1). The observation holds true for two and more fibre crossings. We have also found that for a given diffusion encoding constant and large enough SH series the mapping is unique and thus can be inverted. The inverse mapping can be used to find the closest known solution for $\vec{r}_x$ by using its SH expansion $\boldsymbol{\alpha}_x$.

For the method to work a database of known solutions must first be generated. To create it we select an n number of equally spaced points on a sphere. Since the diffusion is symmetrical only points belonging to the same semi-sphere are needed. Each point on a semi-sphere becomes a phantom fibre direction and for a given b-value, we compute the diffusion signal for all fibre combinations, up to the desired number of fibre crossings K with a preselected combination of volume fractions. We expand the diffusion signal using SHS and store its coefficients along with the fibre configuration.

The size of the final lookup table that can be used to extract the fibre configuration using any arbitrary SH expansion is:

$$\sum_{k=1}^{K} f_k \frac{\prod_{i=1}^{k}(n-i)}{k!}, \tag{7}$$

where f_k is the number of different volume fractions included for a given number of fibre crossings k. When volume fractions are equal, $f_k = 1$.

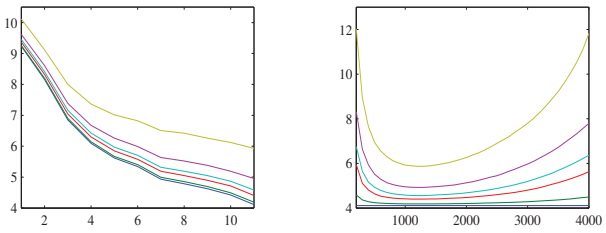
In order to find the fibre configuration using the database, we first expand the diffusion signal with the SHS. There are many potential methods to use the SH coefficients to search the database for the optimal fibre configuration. In this paper, we decided to select the row that minimizes the sum of squared differences between the precomputed and estimated SHS expansion:

$$SSD = \sum_{j=1}^{n}(c_j - \hat{c_j})^2 \tag{8}$$

3. RESULTS

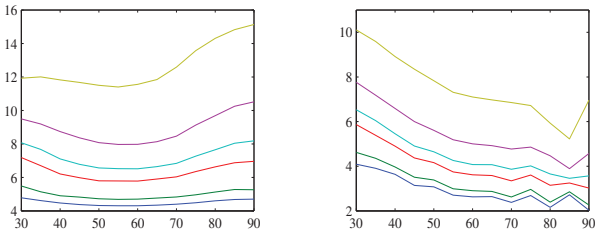
Simulation results using 60 gradient encoding directions are presented in Figures 2, 3 and 4. Figures 2 and 3 show results for one and two fibre configurations respectively and Figure 4 the detection rate of one fibre and two fibre crossing. Unless stated otherwise, the biggest database (#11) was used, b-value was set to 1500, S_0 to 1, and the signal was expanded using the 6th order SHS. Average errors were computed from 10000 iterations. A corrupted signal was created by adding normally distributed random noise, with $\mu = 0$ and $\sigma^2 = 1/\mathrm{SNR}$, to the phantom signal.

The SH expansion of signal from a fibre $\vec{r}_x \subset (\vec{r}_1, \vec{r}_2)$ not present in the database is similar to the expansion of the signal coming from a two fibre crossings $(\vec{r}_1, \vec{r}_2)$ with a small separation angle. Without prior knowledge on the number of fibres the reconstructed multiple fibre crossings with a small separation angle have to be regarded as a single fibre. A good separation angle under which multiple fibre crossings are considered as a single fibre was found as a triple minimal distance between two neighbouring vectors (rounded down to 30 degrees for database #11, Figure 4b).



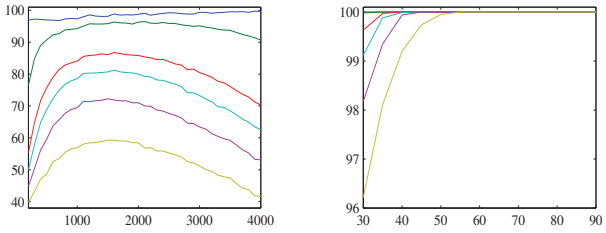
(a) sampling resolution (b) b-value

Fig. 2. Average angular error for 1 fibre depending on: (a) the sampling resolution (see Table 1) and (b) diffusion weighting factor. Lines represent (from bottom) SNR: Inf, 50, 25, 20, 15 and 10.



(a) fibre (b) separation angle

Fig. 3. Average angular error for two fibre crossing, with separation angle ranging from 10 to 90 degrees. Difference between real and resolved (a) fibre and (b) crossing angle. Lines represent (from bottom) SNR: Inf, 50, 25, 20, 15 and 10.



(a) one fibre (b) two fibre crossing

Fig. 4. Detection rate of: (a) one fibre as a function of b-value and (b) two fibre crossing as a function of a separation angle. Lines represent (from top) SNR: Inf, 50, 25, 20, 15 and 10.

4. DISCUSSION

We have presented a novel, scalable method for reconstructing the fibre configurations from HARDI datasets, where the database size, number of resolvable fibre crossings, and included volume fractions can be adjusted. Our method is sensitive enough to resolve the fibre crossings with the separation angle equal to the minimal distance between two neighbouring vectors (Figure 3). The results obtained are comparable to other methods currently used for estimating fibre orientations [12, 19, 13, 21, 22] and could possibly surpass them with a larger database.

As our method uses a discrete representation of the continuous function, the fibre reconstruction accuracy will be dependant on its size (sphere sampling resolution). The shorter the distance between two neighbouring vectors (higher sampling resolution) the more accurate this method becomes (Figure 2a). The average angular error is related to the minimal distance between two neighbouring vectors and the ratio between those two is approximately constant (Table 1). The database with a minimal distance of 2.6 degrees should therefore resolve the fibres with the average angular error of around 1 degree.

Database resolution can be increased by considering more than the one, best solution. Resolved fibres from multiple "good solutions" can be interpolated, resulting in fibre directions that are not present in the database. Additional accuracy can be gained by improving the SNR. Since only part of the SH basis functions contribute to explaining the diffusion signal [23], discarding the statistically insignificant ones should lower the average angular error.

At the moment, when generating the database, we have included all permutations of two fibre crossings. Such a database is therefore highly redundant, as it contains many fibre crossings with the same separation angle. Making it rotation invariant (by rotating the fibres onto a predefined plane and then rotating the solution back) will reduce database size significantly. Finally, a minor reduction can be achieved by utilizing the over-sensitiveness discussed in the Section 3 and removing cases with a low separation angle.

5. REFERENCES

[1] P.J. Basser, J. Mattiello, and D. LeBihan, "MR diffusion tensor spectroscopy and imaging," *Biophysical Journal*, vol. 66, no. 1, pp. 259–267, 1994.

[2] P.J. Basser, J. Mattiello, and D. LeBihan, "Estimation of the effective self-diffusion tensor from the NMR spin echo," *Journal of Magnetic Resonance Series B*, vol. 103, no. 3, pp. 247–254, 1994.

[3] D.K. Jones, "The effect of gradient sampling schemes on measures derived from diffusion tensor MRI: A monte carlo study," *Magnetic Resonance in Medicine*, vol. 51, no. 4, pp. 807–815, 2004.

[4] D.K. Jones, M.A. Horsfield, and A Simmons, "Optimal strategies for measuring diffusion in anisotropic systems by magnetic resonance imaging," *Magnetic Resonance in Medicine*, vol. 42, no. 3, pp. 515–525, 1999.

[5] K.M. Hasan, D.L. Parker, and A.L. Alexander, "Comparison of gradient encoding schemes for diffusion-tensor MRI," *Journal of Magnetic Resonance Imaging*, vol. 13, no. 5, pp. 769–780, 2001.

[6] D.C. Alexander, G.J. Barker, and S.R. Arridge, "Detection and modeling of non-gaussian apparent diffusion coefficient profiles in human brain data," *Magnetic Resonance in Medicine*, vol. 48, no. 2, pp. 331–340, 2002.

[7] L.R. Frank, "Characterization of anisotropy in high angular resolution diffusion-weighted MRI," *Magnetic Resonance in Medicine*, vol. 47, pp. 1083–1099, 2002.

[8] A.W. Anderson, "Measurement of fiber orientation distributions using high angular resolution diffusion imaging," *Magnetic Resonance in Medicine*, vol. 54, no. 5, pp. 1194–1206, 2005.

[9] A.L. Alexander, K.M. Hasan, M. Lazar, J.S. Tsuruda, and D.L. Parker, "Analysis of partial volume effects in diffusion-tensor MRI," *Magnetic Resonance in Medicine*, vol. 45, no. 5, pp. 770–780, 2001.

[10] D.S. Tuch, T.G. Reese, M.R. Wiegell, N. Makris, J.W. Belliveau, and V.J. Wedeen, "High angular resolution diffusion imaging reveals intravoxel white matter fiber heterogeneity," *Magnetic Resonance in Medicine*, vol. 48, no. 4, pp. 577–582, 2002.

[11] L.R. Frank, "Anisotropy in high angular resolution diffusion-weighted mri," *Magnetic Resonance in Medicine*, vol. 45, pp. 935–939, 2001.

[12] B.W. Kreher, J.F. Schneider, I. Mader, E. Martin, J. Hennig, and K.A. Il'yasov, "Multitensor approach for analysis and tracking of complex fiber configurations," *Magnetic Resonance in Medicine*, vol. 54, no. 5, pp. 1216–1225, 2005.

[13] S. Peled, O. Friman, F. Jolesz, and C.F. Westin, "Geometrically constrained two-tensor model for crossing tracts in DWI," *Magnetic Resonance Imaging*, vol. 24, no. 9, pp. 1263–1270, 2006.

[14] E. Özarslan and T.H. Mareci, "Generalized diffusion tensor imaging and analytical relationships between diffusion tensor imaging and high angular resolution diffusion imaging," *Magnetic Resonance in Medicine*, vol. 50, no. 5, pp. 955–965, 2003.

[15] J.D. Tournier, F. Calamante, D.G. Gadian, and A. Connelly, "Direct estimation of the fiber orientation density function from diffusion-weighted MRI data using spherical deconvolution," *NeuroImage*, vol. 23, no. 3, pp. 1176–1185, 2004.

[16] J.D. Tournier, F. Calamante, and A. Connelly, "Robust determination of the fibre orientation distribution in diffusion MRI: non-negativity constrained super-resolved spherical deconvolution," *NeuroImage*, vol. 35, no. 4, pp. 1459–1472, 2007.

[17] D.S. Tuch, T.G. Reese, M.R. Wiegell, and V.J. Wedeen, "Diffusion MRI of complex neural architecture," *Neuron*, vol. 40, no. 5, pp. 885–895, 2003.

[18] D.S. Tuch, "Q-ball imaging," *Magnetic Resonance in Medicine*, vol. 52, no. 6, pp. 1358–1372, 2004.

[19] E. Özarslan, T.M. Shepherd, B.C. Vemuri, S.J. Blackband, and T.H. Mareci, "Resolution of complex tissue microarchitecture using the diffusion orientation transform (DOT)," *NeuroImage*, vol. 31, no. 3, pp. 1086–1103, 2006.

[20] K.M. Jansons and D.C. Alexander, "Persistent angular structure: new insights from diffusion magnetic resonance imaging data," *Inverse Problems*, vol. 19, pp. 1031, 2003.

[21] B. Jian, B.C. Vemuri, E. Özarslan, P.R. Carney, and T.H. Mareci, "A novel tensor distribution model for the diffusion-weighted MR signal," *NeuroImage*, vol. 37, no. 1, pp. 164–176, 2007.

[22] V. Prčkovska, AF Roebroeck, WL Pullens, A. Vilanova, and R.B.M. ter Haar, "Optimal acquisition schemes in high angular resolution diffusion weighted imaging," in *Medical Image Computing and Computer-Assisted Intervention*, 2008, vol. 11, p. 9.

[23] B.P. Neuman, L. Bai, and C. Tench, "Reliably estimating the diffusion orientation distribution function from high angular resolution diffusion imaging data," in *Medical Image Understanding and Analysis*, 2011.